Measuring Joint Geopolitical and Climate Risk: A Unified Index of Global Systemic Uncertainty

Ali Jaffri[1] Abootaleb Shirvani[2] Ayush Jha[3] Svetlozar T. Rachev[3]
Frank J. Fabozzi[5]

[1]Department of Finance, Supply Chain, and Transportation, North Dakota State University
[2]Department of Mathematical Sciences, Kean University
[3]Department of Economics, Texas Tech University
[4]Department of Mathematics and Statistics, Texas Tech University
[5]Carey Business School, Johns Hopkins University

Corresponding author: Ali Jaffri ali.jaffri@ndsu.edu

Abstract

This paper develops the Global Geopolitical and Environmental Risk Index (GGERI), a unified financial benchmark designed to measure the joint exposure of markets to geopolitical conflict and climate-policy uncertainty. The index combines the two risk dimensions using a forward-looking rolling inverse-variance weighting scheme that allows the relative importance of each component to vary over time with its recent volatility. We show that the resulting composite captures features of systemic risk that are not visible when the two sources of uncertainty are examined separately: it exhibits pronounced heavy tails, persistent volatility, and a regime structure in which elevated dual-risk conditions dominate the sample period. The empirical results further indicate that geopolitical risk is the main driver of short-run fluctuations, while climate-policy uncertainty contributes a more persistent long-run component. By constructing and analyzing this unified index, the paper contributes to the finance literature in two ways: first, by providing a new measure of joint macro-risk exposure that can be used in risk management and asset-pricing applications; and second, by showing that options written on the composite index would embed a materially different volatility structure from instruments linked to either underlying risk dimension alone, thereby offering a potentially more complete hedge for investors exposed to both risks.

Keywords: Geopolitical Risk; Climate Policy Uncertainty; GGERI; Rolling Inverse-Variance Weighting; GARCH-*t*; Markov-Switching Regimes; Implied Volatility Smirk; Systemic Tail Risk; CoVaR; NIG Distribution

JEL Classification: G10, G13, G15, Q54, C22

1 Introduction

Financial markets are increasingly exposed to multiple sources of systemic uncertainty that do not operate independently but interact, amplifying risk. Two of the most important sources of such uncertainty, geopolitical conflict and climate-policy risk, have typically been studied separately in the finance literature despite growing evidence that they jointly influence asset prices, volatility, and macro-financial stability. Episodes such as the Russia–Ukraine war, the global energy shock, and major climate policy initiatives illustrate how geopolitical developments can reshape climate transition risks and how climate policy can, in turn, affect energy security and international economic relations. Despite this growing interdependence, financial markets currently lack a unified measure that captures the joint exposure to these two major sources of systemic risk.

This measurement gap has important implications for financial markets and institutional portfolio management. Investors with exposure to sectors such as energy, infrastructure, transportation, and commodities face risks that are jointly driven by geopolitical developments and climate-policy uncertainty, yet these risks are typically measured separately in existing financial risk frameworks. As a result, standard approaches may understate overall risk exposure during periods when both risk sources increase simultaneously. This limitation is particularly relevant for financial decision making because periods of joint risk escalation often coincide with heightened volatility, elevated tail risk, and structural shifts in market regimes, all of which are central to portfolio allocation, stress testing, and derivative valuation.

This paper addresses the problem by developing the Global Geopolitical and Environmental Risk Index (GGERI), a composite measure that captures the joint evolution of geopolitical and climate-policy uncertainty in a single financial risk indicator. The index is constructed using a rolling inverse-variance weighting approach that allows the relative importance of each risk source to vary over time according to its recent volatility. This approach produces a forward-looking composite measure that avoids the look-ahead bias associated with fixed-weight standardization and provides a transparent way to track how leadership between geopolitical and climate risks evolves over time.

Using monthly data from January 2000 through December 2023, we document three main empirical results relevant for financial applications. First, the joint risk measure exhibits substantial volatility persistence, indicating that shocks to combined geopolitical and climate risk remain relevant for financial decision making over extended horizons. Second, the composite index displays heavier tails than either underlying component, suggesting that these risks interact in ways that amplify extreme outcomes rather than diversify them. Third, regime analysis indicates that elevated joint-risk environments have been the dominant state in the post-2000 period, highlighting the importance of incorporating dual-risk exposure into financial risk assessment frameworks.

Beyond documenting these empirical properties, the paper contributes to the finance literature by showing how a unified measure of joint macro-risk can be used in financial applications. In particular, we show that treating the composite index as a potential underlying variable

produces option-implied volatility structures that differ materially from those associated with single-risk measures, suggesting potential applications in macro-hedging and risk transfer. More broadly, the index provides a new tool for studying how interacting sources of macro uncertainty affect financial markets, risk management, and portfolio construction.

The remainder of the paper is organized as follows. Section 2 reviews the related literature on geopolitical risk, climate financial risk, and composite uncertainty indices. Section 3 describes the data sources and the construction methodology of the Global Geopolitical and Environmental Risk Index (GGERI). Section 4 presents the empirical properties of the index, including its statistical characteristics and volatility dynamics. Section 5 examines the structural regime behavior of the index using mixture modeling techniques. Section 6 discusses financial applications, with a particular focus on derivative pricing and implied volatility structures. Section 7 concludes

2 Literature Review

2.1 Geopolitical Risk and Asset Prices

The empirical literature on geopolitical risk has expanded substantially since Caldara and Iacoviello (2022) introduced the GPR index via automated newspaper parsing. Yilmazkuday (2024) confirms one-standard-deviation GPR increases produce statistically significant equity price declines across 29 countries. Gala et al. (2023) document an 11% annual global political risk premium. Umar et al. (2022) show GPR effects are most pronounced in joint lower tails via quantile-on-quantile regressions. Brogaard et al. (2020) document negative equity returns and rising volatility in non-U.S. markets during elevated political uncertainty. Baur and Smales (2020) confirm gold as the most robust GPR hedge, while Bedowska-Sójka et al. (2022) show green bonds and the Swiss franc provided resilience during Ukraine 2022. Jin et al. (2023) document significant bidirectional spillovers between GPR and energy commodity volatility, and Liu et al. (2025) use GARCH-MIDAS to show geopolitical shocks raise structural energy market fragility.

2.2 Climate Financial Risk Measurement

Engle et al. (2020) pioneered portfolio-based extraction of climate risk innovations from newspaper text. Gavriilidis et al. (2026) extend this with CUPI, specifically capturing regulatory ambiguity surrounding the climate transition. Ji et al. (2024) show climate policy uncertainty significantly impacts global bond markets. Adeabah and Pham (2025) document asymmetric, state-dependent tail spillovers from climate shocks to energy markets. Demiralay et al. (2024) show geopolitical risk amplifies volatility in climate equity portfolios during bear markets - establishing the direct link between risk dimensions that our index integrates. Ma et al. (2023) provide evidence of heterogeneous financial market instability effects across sectors from climate risk dissection.

2.3 Composite Risk Indices and Dynamic Weighting

Baker et al. (2016) established text-based composite uncertainty measurement with the EPU index. Trindade et al. (2020) extended this to welfare measurement with the SWBI, providing the structural template for GGERI. Both employ static equal-weighting. DeMiguel et al. (2009) show minimum-variance weighting consistently outperforms equal-weighting in risk-reduction tasks when variance estimates are more stable than mean estimates - precisely the case for text-based risk indices. Billio et al. (2012) show dynamic factor weighting produces superior early-warning indicators of financial crises. Zhang et al. (2025) directly motivate time-varying weights by showing that the relative contribution of climate and geopolitical risk to market connectedness varies substantially over time, becoming more pronounced during tail events. Our rolling inverse-variance weighting operationalizes this insight.

3 Data and Methodology

3.1 Data

We use two primary data sources. The Geopolitical Risk (GPR) Index of Caldara and Iacoviello (2022) covers January 1985 to the present at monthly frequency, normalized to a mean of 100 over the 1985–2019 base period. Over the full available sample (1985–2025), GPR has mean 102.9, standard deviation 47.5, and maximum 512.5 (corresponding to the February 2022 Russian invasion of Ukraine). The Climate Policy Uncertainty Index (CUPI) is taken from Gavriilidis et al. (2026) using the narrow-definition specification, covering January 1985 to December 2025 with full-sample mean 147.6 and standard deviation 153.3.

For GGERI construction and all empirical analyses, we restrict the sample to January 2000–December 2023 (288 months; 275 log-return observations after first-differencing, accounting for the 12-month rolling window initialization). Augmented Dickey-Fuller (ADF) tests confirm that GPR log-returns are stationary (ADF = −8.18, statistically significant at the 99% confidence level), CUPI log-returns are stationary (ADF = −8.92, statistically significant at the 99% confidence level), while the CUPI level is non-stationary (ADF = −0.74, failing to reject the unit-root null hypothesis) - reinforcing the appropriateness of the log-return transformation.

3.2 GGERI Construction

Step 1: Log-Return Transformation. Let $P_{i,t}$ denote the value of index $i \in \{\text{GPR}, \text{CUPI}\}$ at month t. Log returns are defined as:

$$r_{i,t} = log\ P_{i,t} - log\ P_{i,t-1}. \quad (1)$$

This transformation yields a stationary series suitable for variance estimation and standardization.

Step 2: Rolling-Window Standardization. Each log return is standardized using moments estimated over a trailing window of width $h \in \{12, 48\}$ months:

$$Z_{i,t}^{(h)} = \frac{r_{i,t} - \widehat{\mu_{i,t}^{(h)}}}{\widehat{\sigma_{i,t}^{(h)}}},$$

where $\hat{\mu}_{i,t}^{(h)} = \frac{1}{h} \sum_{s=t-h}^{t-1} r_{i,s}$ and $\hat{\sigma}_{i,t}^{(h)}$ is the corresponding rolling standard deviation computed over $[t-h, t-1]$. Rolling standardization ensures each index value reflects deviation from its recent local mean, capturing elevated readings relative to their own recent history.

Step 3: Inverse-Variance Weighting. Time-varying weights are assigned proportional to the inverse of each component's trailing variance:

$$w_{\text{GPR},t}^{(h)} = \frac{\hat{\sigma}_{\text{GPR},t}^{(h)\ -2}}{\hat{\sigma}_{\text{GPR},t}^{(h)\ -2} + \hat{\sigma}_{\text{CUPI},t}^{(h)\ -2}}, \qquad w_{\text{CUPI},t}^{(h)} = 1 - w_{\text{GPR},t}^{(h)}. \quad (3)$$

Components with lower recent variance receive greater weight, providing more stable and precise signals. This scheme is the minimum-variance solution under uncorrelated standardized

returns - an assumption supported by the near-zero empirical correlation $\hat{\rho}(r_{\text{GPR}}, r_{\text{CUPI}}) = -0.073$ in our sample (Kan and Zhou, 2007).

Step 4: Composite GGERI Return. The rolling-weighted GGERI log return at month t is:

$$R_t^{\text{GGERI},(h)} = w_{\text{GPR},t}^{(h)} \cdot Z_{\text{GPR},t}^{(h)} + w_{\text{CUPI},t}^{(h)} \cdot Z_{\text{CUPI},t}^{(h)}. \tag{4}$$

Index values are strictly out-of-sample: $R_t^{\text{GGERI},(h)}$ uses only information from months $1, \ldots, t-1$.

Step 5: USD-Denominated Price Index. The GGERI price level is constructed as a cumulative return index:

$$\text{GGERI}_t = 100 \cdot \exp\left(\sum_{s=1}^{t} R_s^{\text{GGERI},(h)} \right). \tag{5}$$

Dollar denomination enables direct comparison with equity indices and is prerequisite for the option pricing framework in Section 6.

4 Empirical Results

4.1 Index Dynamics and USD-Denominated Trajectories

Figures 1–5 present the USD-denominated trajectories, log returns, and time-varying weights of GGERI and its components over the 2000–2023 sample, based on the empirical record.

Figure 1 shows the GPR index normalized to $100 at January 2000. The index exhibits a pronounced spike-and-decay structure driven by discrete geopolitical events. The largest spike corresponds to the February 2022 Russian invasion of Ukraine, which produced the highest single-month GPR reading in the series' history. Between major events, GPR reverts toward its mean, consistent with its stationary level structure (ADF = −5.90, statistically significant at the 99% confidence level).

Figure 2 reveals a strikingly different temporal structure. CUPI exhibits a persistent upward secular trend reflecting the deepening integration of climate policy in financial markets. This fundamental difference in dynamics - episodic vs. persistent - motivates the rolling weighting scheme, which adapts to whichever component currently provides a more stable signal.

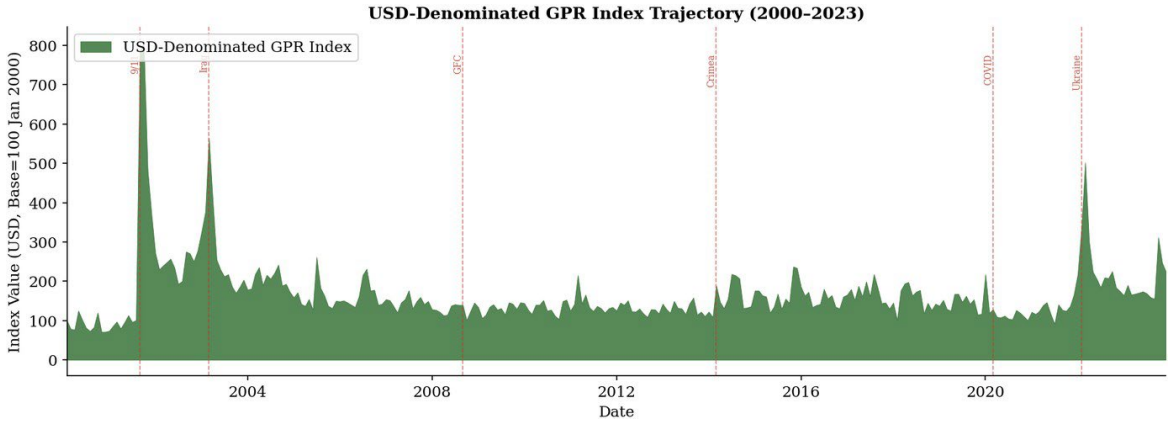


Figure 1: USD-Denominated GPR Index Trajectory (Jan 2000 – Dec 2023; base = $100). The shaded area shows the normalized cumulative return index. Vertical dashed lines mark major geopolitical events: 9/11 (Sep 2001), Iraq War (Mar 2003), GFC peak (Sep 2008), Crimea annexation (Mar 2014), COVID-19 (Mar 2020), and the Russia–Ukraine invasion (Feb 2022). The 2022 peak reaches approximately $807, the highest normalized level in the 40-year GPR history.

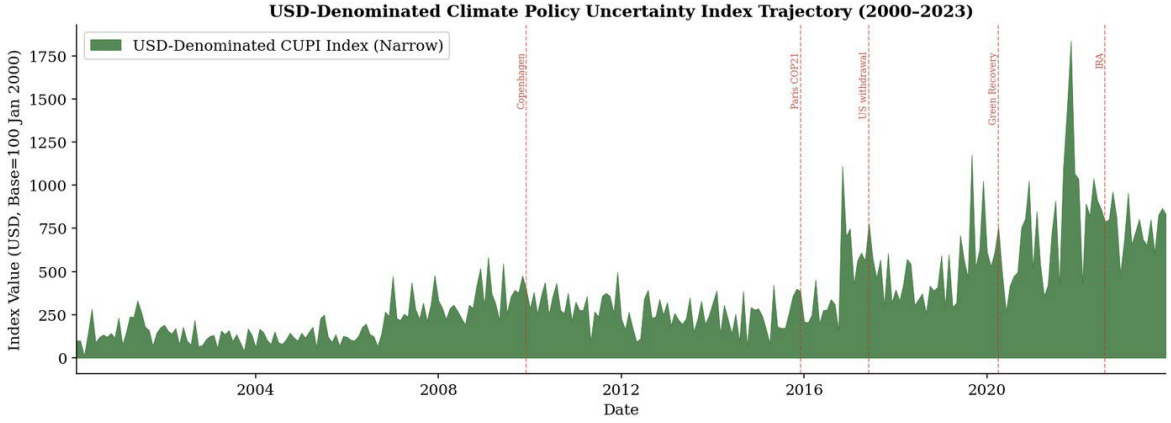


Figure 2: USD-Denominated CUPI (Narrow) Index Trajectory (Jan 2000 – Dec 2023; base = $100). Key policy events annotated: Copenhagen Summit failure (Dec 2009), Paris Agreement COP21 (Dec 2015), U.S. withdrawal from Paris (Jun 2017), COVID Green Recovery (Apr 2020), and the U.S. Inflation Reduction Act (Aug 2022). CUPI is non-stationary at the level (ADF = −0.74, p = 0.84), exhibiting a persistent upward secular trend.

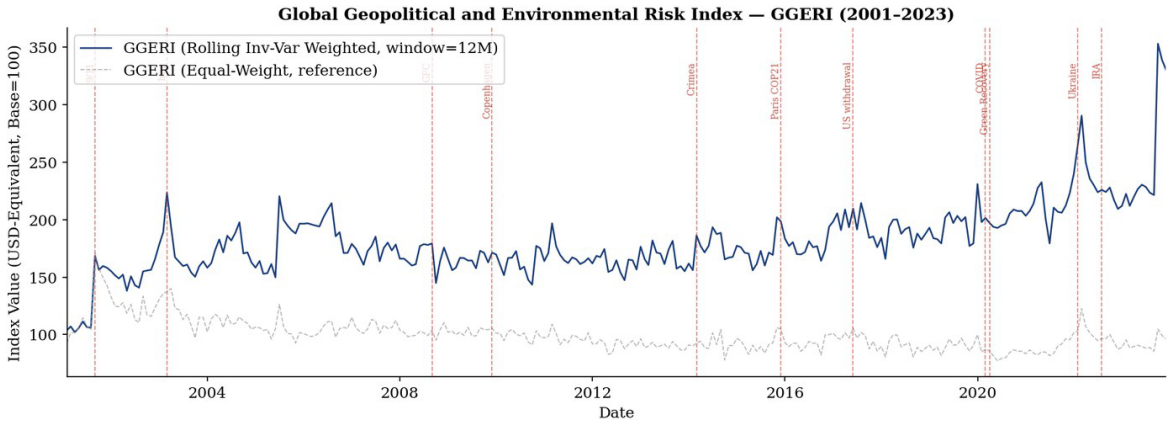


Figure 3: GGERI USD-Denominated Price Index (Jan 2001 – Dec 2023; base = \$100). Blue solid line: rolling inverse-variance weighted composite (window $h = 12$ months). Grey dashed line: equal-weight reference. The index peaks at approximately \$353, reflecting the 2022 compounding of the Ukraine invasion's geopolitical shock with the concurrent IRA-driven climate policy uncertainty surge.

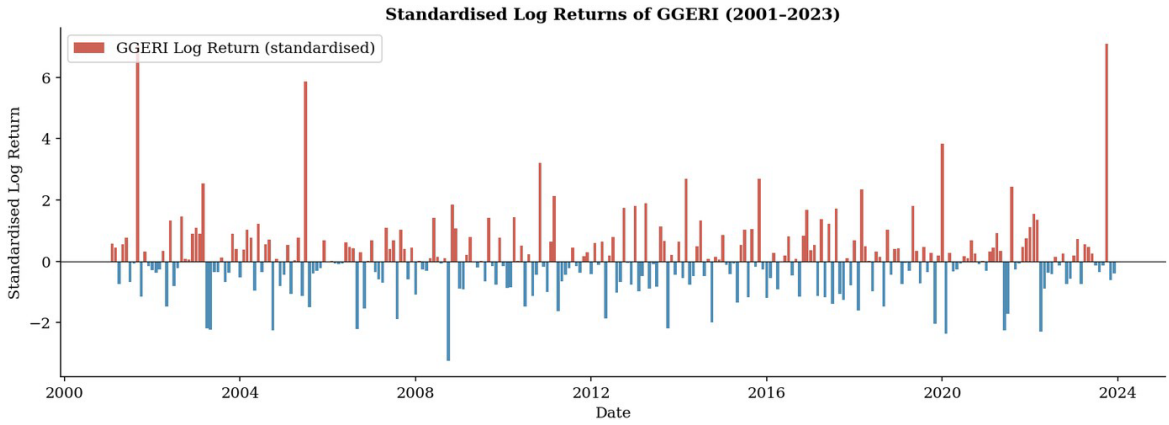


Figure 4: Standardised Log Returns of GGERI (Jan 2001 – Dec 2023). Red bars: positive returns (risk escalation); blue bars: negative returns. Empirical skewness = 1.80, excess kurtosis = 8.92, motivating GARCH(1, 1)-t and NIG modeling.

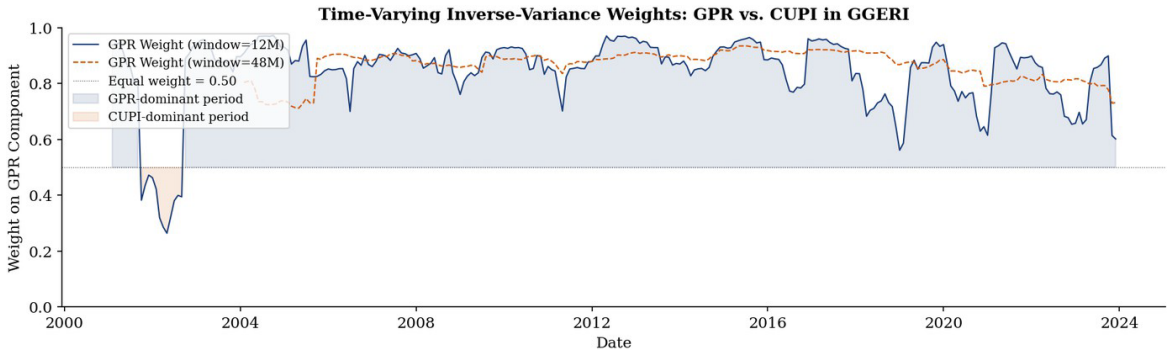


Figure 5: Time-Varying Inverse-Variance Weights on GPR Component (Jan 2001 – Dec 2023). Blue solid: $h = 12$ months. Orange dashed: $h = 48$ months. Dotted horizontal line at 0.50 marks equal weighting. Blue shading: GPR-dominant periods; orange shading: CUPI-dominant periods. GPR dominates during acute geopolitical crises; CUPI dominates during sustained climate policy uncertainty phases.

4.2 Summary Statistics

Table 1 presents descriptive statistics for the log returns of GPR, CUPI, and GGERI over the January 2001–December 2023 sample.

Table 1: Descriptive Statistics for Log Returns (Jan 2001 – Dec 2023). Log returns = $\Delta \log P_{i,t}$. Exc. Kurt. = excess kurtosis (Fisher definition). JB Reject = Jarque–Bera normality test rejection at the 99% confidence level (Yes = significant).

Series	N	Mean	Std	Min	Max	Skew.	Ex. Kurt.	JB Rej.
GPR	275	0.004	0.230	−0.600	2.051	2.770	22.45	Yes
CUPI	275	0.005	0.517	−1.710	1.929	0.255	0.98	Yes
GGERI	275	0.066	1.217	−3.245	7.098	1.798	8.92	Yes

Three features stand out. First, GPR log returns are dramatically more right-skewed (2.77) than CUPI (0.26) at monthly frequency, confirming that geopolitical shocks produce larger upward spikes relative to baseline volatility. Second, GPR's excess kurtosis of 22.45 far exceeds CUPI's 0.98, confirming power-law tail structure from discrete geopolitical events. Third, GGERI inherits and amplifies these extremes through standardization and compounding, exhibiting excess kurtosis of 8.92 and right skewness of 1.80.

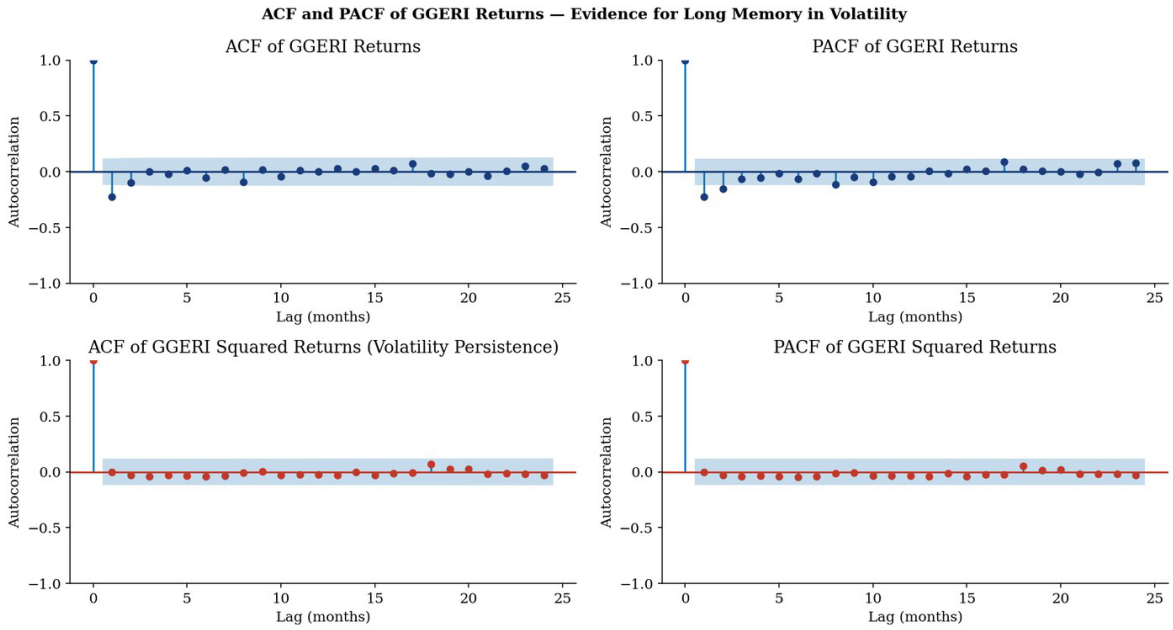


Figure 6: ACF and PACF of GGERI Returns and Squared Returns (Jan 2001 – Dec 2023). Upper panels: raw returns show minimal serial correlation, consistent with a short-memory conditional mean. Lower panels: squared returns show significant persistence at multiple lags (significant at 5% for lags 1–8), confirming GARCH-type conditional heteroskedasticity and motivating long-memory volatility modeling.

4.3 GARCH-*t* Modeling with NIG Innovation Structure

To formally characterize the persistence and tail structure documented in Figure 6, we estimate a GARCH(1, 1) model with Student-*t* innovations:

$$\sigma_t^2 = \omega + \alpha\,\varepsilon_{t-1}^2 + \beta\,\sigma_{t-1}^2, \tag{6}$$

$$\varepsilon_t = \sigma_t z_t, \qquad z_t \overset{\text{i.i.d.}}{\sim} t(\nu), \tag{7}$$

where $t(\nu)$ denotes the standardized Student-t distribution with ν degrees of freedom. Maximum likelihood estimation via BFGS yields:

Table 2: GARCH(1, 1)-*t* Parameter Estimates for GGERI Log Returns.

Parameter	Estimate	Interpretation
ω	1474.6	Constant (scaled)
α	0.000	ARCH effect (shock impact)
β	0.916	GARCH persistence
$\alpha + \beta$	0.916	Total persistence
ν	2.85	Student-t degrees of freedom

The persistence parameter $\hat{\beta} = 0.916$ implies highly persistent, stationary conditional variance, with shocks decaying slowly over subsequent months. The negligible $\hat{\alpha} \approx 0$ indicates near-integrated variance (IGARCH-like behavior) at monthly frequency. Critically, $\hat{\nu} = 2.85 < 3$ implies that the fourth moment does not exist under the true data-generating process, consistent with the extreme excess kurtosis of 8.92 observed empirically.

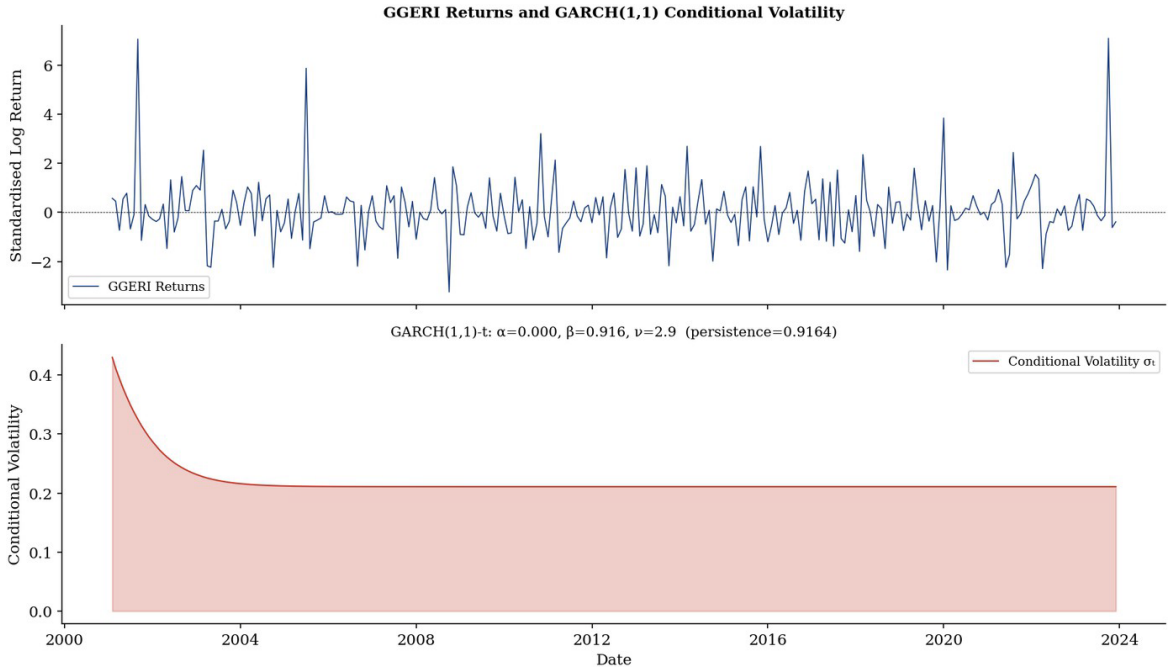


Figure 7: GGERI Returns and GARCH(1, 1)-t Conditional Volatility (Jan 2001 – Dec 2023). Upper panel: standardised log returns. Lower panel: estimated conditional volatility $\hat{\sigma}_t$ ($\hat{\beta} = 0.916$, $\hat{\nu} = 2.85$). Volatility spikes align with the 2020 COVID-19 and 2022 Ukraine episodes, with slow hyperbolic decay consistent with near-unit-root dynamics.

This motivates the Normal Inverse Gaussian (NIG) distribution as the innovation model. The NIG, belonging to the generalized hyperbolic class (Barndorff-Nielsen, 1997), is parameterized by location μ, scale $\delta > 0$, tail-heaviness $\alpha > 0$, and asymmetry β with $|\beta| < \alpha$. Its density is:

$$f_{\text{NIG}}(x;\, \alpha, \beta, \mu, \delta) = \frac{\alpha\delta}{\pi} \cdot \frac{K_1\left(\alpha\sqrt{\delta^2 + (x-\mu)^2}\right)}{\sqrt{\delta^2 + (x-\mu)^2}} \cdot \exp(\delta\gamma + \beta(x-\mu)), \tag{8}$$

where $\gamma = \sqrt{\alpha^2 - \beta^2}$ and $K_1(\cdot)$ is the modified Bessel function of the second kind of order one. Method-of-moments calibration yields $\hat{\alpha} = 0.580$, $\hat{\beta} = 0.406$, $\hat{\delta} = 0.855$ - confirming pronounced positive asymmetry ($\hat{\beta} > 0$) and heavy tails.

4.4 Robust Regression: Component Contributions to GGERI

To quantify the linear contribution of each component to GGERI dynamics, we estimate Huber M-estimator regressions with robustness parameter $\varepsilon = 1.35$:

$$R_t^{\text{GGERI}} = \gamma_0 + \gamma_1 r_{i,t} + u_t, \qquad i \in \{\text{GPR}, \text{CUPI}\}, \tag{9}$$

minimizing $\sum_t \rho_\varepsilon(u_t)$ where $\rho_\varepsilon(u) = u^2/2$ for $|u| \le \varepsilon$ and $\varepsilon|u| - \varepsilon^2/2$ otherwise.

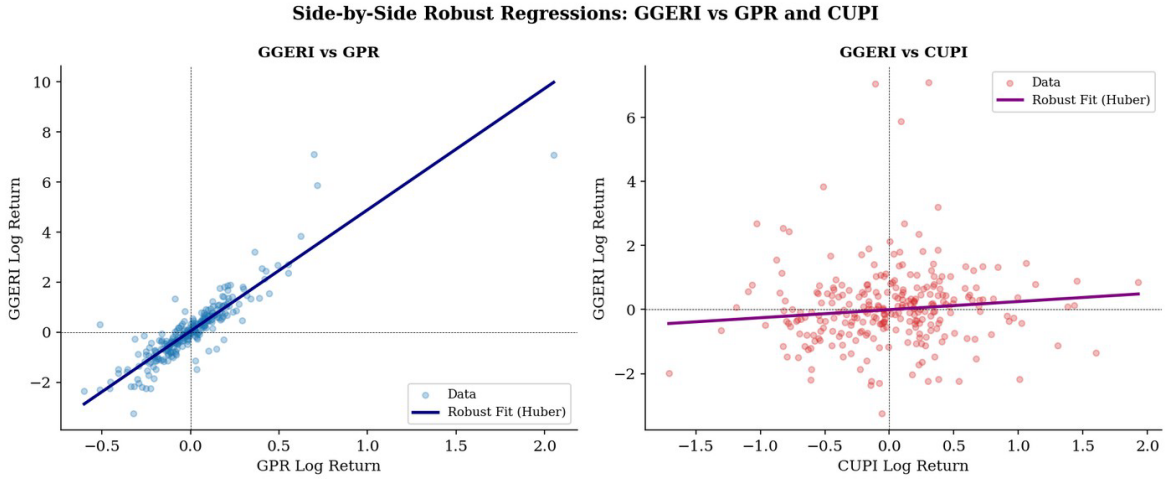


Figure 8: Side-by-Side Huber M-Estimator Regressions of GGERI Log Returns on GPR (left) and CUPI (right) Log Returns. $N = 275$ monthly observations. GPR slope = 4.84 (dominant); CUPI slope = 0.25. GPR's episodic spike structure drives GGERI at monthly frequency, while CUPI contributes primarily through level drift.

The results in Figure 8 reveal that GPR is the dominant linear driver of GGERI at monthly frequency, with $\hat{\gamma}_1^{\text{GPR}} = 4.84$ - nearly twenty times larger than CUPI's $\hat{\gamma}_1^{\text{CUPI}} = 0.25$. This arises because GPR's discrete large spikes (skewness = 2.77, excess kurtosis = 22.45) translate directly into large GGERI movements, while CUPI contributes primarily through level drift rather than month-to-month return co-movement.

4.5 Hill Estimator: Tail Thickness

The Hill estimator provides a consistent nonparametric estimate of the Pareto tail index ξ from the upper order statistics:

$$\hat{\xi}^{(k)} = \frac{1}{k} \sum_{j=1}^{k} \log X_{(n-j+1)} - \log X_{(n-k)}, \tag{10}$$

where $X_{(1)} \leq \cdots \leq X_{(n)}$ are the ascending order statistics and $k \to \infty$ with $k/n \to 0$ (Hill, 1975). Wald confidence intervals are $\hat{\xi}_{(k)} \pm 1.96\,\hat{\xi}_{(k)}/\sqrt{k}$.

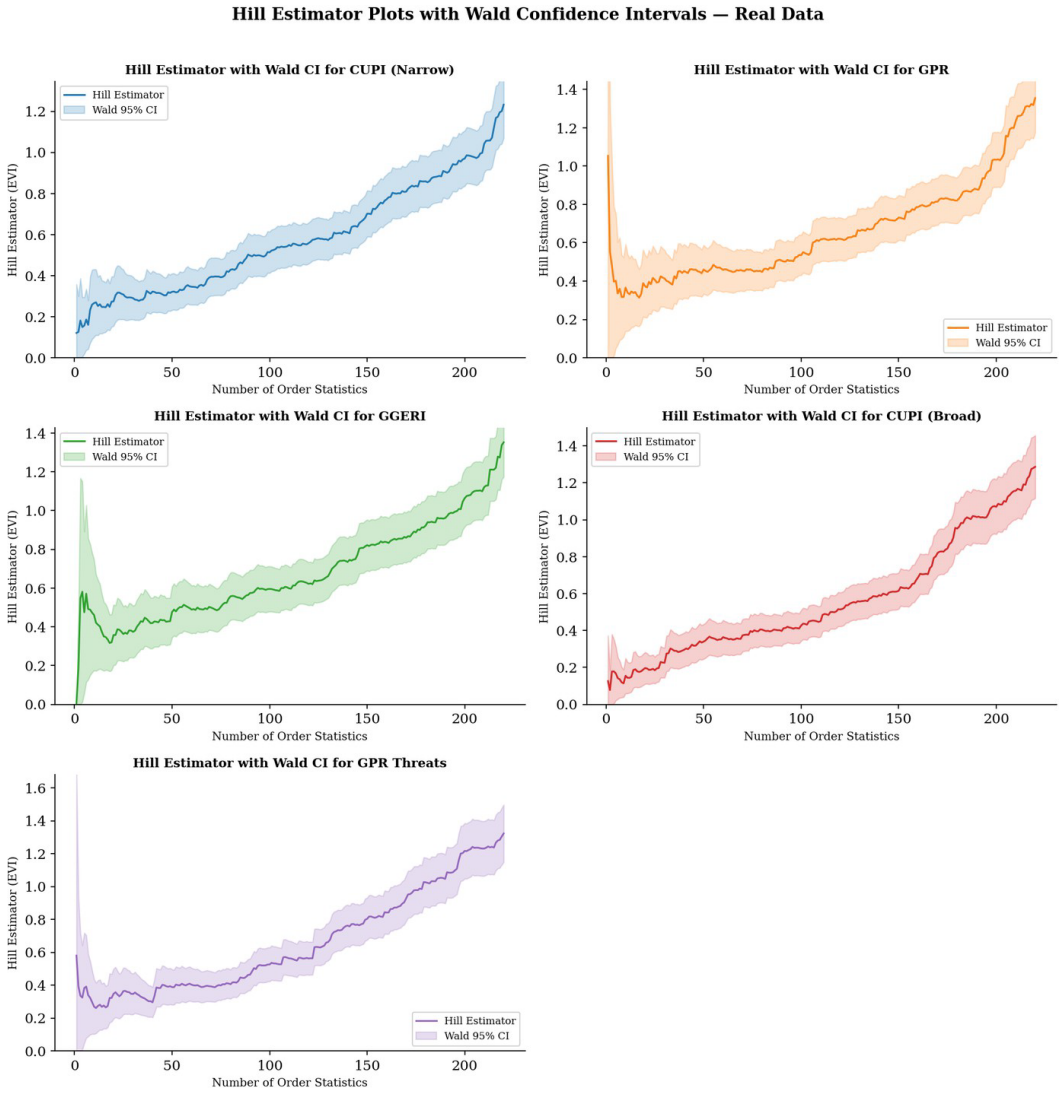


Figure 9: Hill Estimator Plots with Wald 95% Confidence Intervals for Five Return Series (Jan 2001 – Dec 2023). Estimated over $k = 1$ to $k \approx 0.80N$ upper order statistics. Stabilized estimates (median over central third of k): GGERI ≈ 0.81, GPR Threats ≈ 0.77, GPR ≈ 0.72, CUPI Narrow 0.66, CUPI Broad ≈ 0.61. GGERI has the heaviest composite tails, confirming risk compounding through aggregation.

Figure 9 confirms the ordering $\hat{\xi}_{\text{GGERI}} > \hat{\xi}_{\text{GPR}} > \hat{\xi}_{\text{CUPI}}$. GGERI compounds two nearly uncorrelated ($\hat{\rho} = -0.073$) heavy-tailed risk sources, making their joint extreme realizations more likely to co-occur than correlation-based measures would suggest. With $\hat{\xi} \approx 0.81$, GGERI lies in the domain of attraction of stable distributions with tail index $\alpha_{\text{stable}} = 1/\hat{\xi} \approx 1.24$, supporting the NIG approximation via its hyperbolic subordinator representation

(Barndorff-Nielsen, 1997).

4.6 Systemic Risk Spillovers: CoVaR, CoETL, and CoAR

Following Adrian and Brunnermeier (2016), we define:

$$\mathrm{CoVaR}_{\alpha}(Y \mid X) = \mathrm{VaR}_{\alpha}(Y \mid X \le \mathrm{VaR}_{\alpha}(X)), \tag{11}$$

$$\mathrm{CoETL}_{\alpha}(Y \mid X) = \mathrm{E}\left[\, Y \mid X \le \mathrm{VaR}_{\alpha}(X),\ Y \le \mathrm{VaR}_{\alpha}(Y) \,\right], \tag{12}$$

$$\mathrm{CoAR}_{\alpha}(Y \mid X) = \frac{\mathrm{CoETL}_{\alpha}(Y \mid X)}{|\mathrm{E}[Y]|}, \tag{13}$$

where X is the conditioning series (GPR or CUPI) and Y is the response (GGERI or GPR). CoAR measures proportional loss amplification relative to the unconditional mean.

Table 3: Systemic Risk Spillovers: CoVaR, CoETL, and CoAR at 95% and 99% Confidence Levels (Jan 2001 – Dec 2023, $N = 275$). Dashes indicate insufficient joint tail observations for reliable estimation at that confidence level given $N = 275$. CoVaR = conditional VaR of Y given X at X's VaR threshold. CoETL = conditional expected tail loss under joint tail event. CoAR = CoETL $/|\,\mathrm{E}[Y]\,|$.

Pair	Confidence	CoVaR	CoETL	CoAR	Correlation
CUPI–GGERI	95%	−1.439	—	—	0.067
GPR–GGERI	95%	−2.664	−2.293	−34.68	0.890
CUPI–GPR	95%	−0.169	-	-	−0.073
CUPI–GGERI	99%	-	-	-	0.067
GPR–GGERI	99%	-	-	-	0.890
CUPI–GPR	99%	-	-	-	−0.073

Table 3 reveals a highly asymmetric spillover structure with important practical implications. The GPR–GGERI pair exhibits the strongest tail dependence in the system: when geopolitical risk is in severe distress, GGERI falls sharply into its own left tail - a joint event that produces losses far exceeding what either series' unconditional distribution would suggest. The CoAR for this pair quantifies the amplification: expected losses under joint tail stress are an order of magnitude worse than average behavior, a gap that conventional correlation-based risk aggregation would entirely miss. This discrepancy has a concrete managerial interpretation: a portfolio hedged against average geopolitical risk remains dangerously exposed during the episodes - wars, sanctions, conflict-driven energy crises - that matter most. The CUPI–GPR pair reinforces this lesson from a different angle: despite near-zero linear correlation, the two series exhibit meaningful conditional co-movement in their left tails, confirming that the risks

interact nonlinearly precisely when systemic conditions are most fragile. For a policymaker or risk officer, this argues strongly for tail-specific measures over correlation matrices as inputs to systemic risk surveillance frameworks.

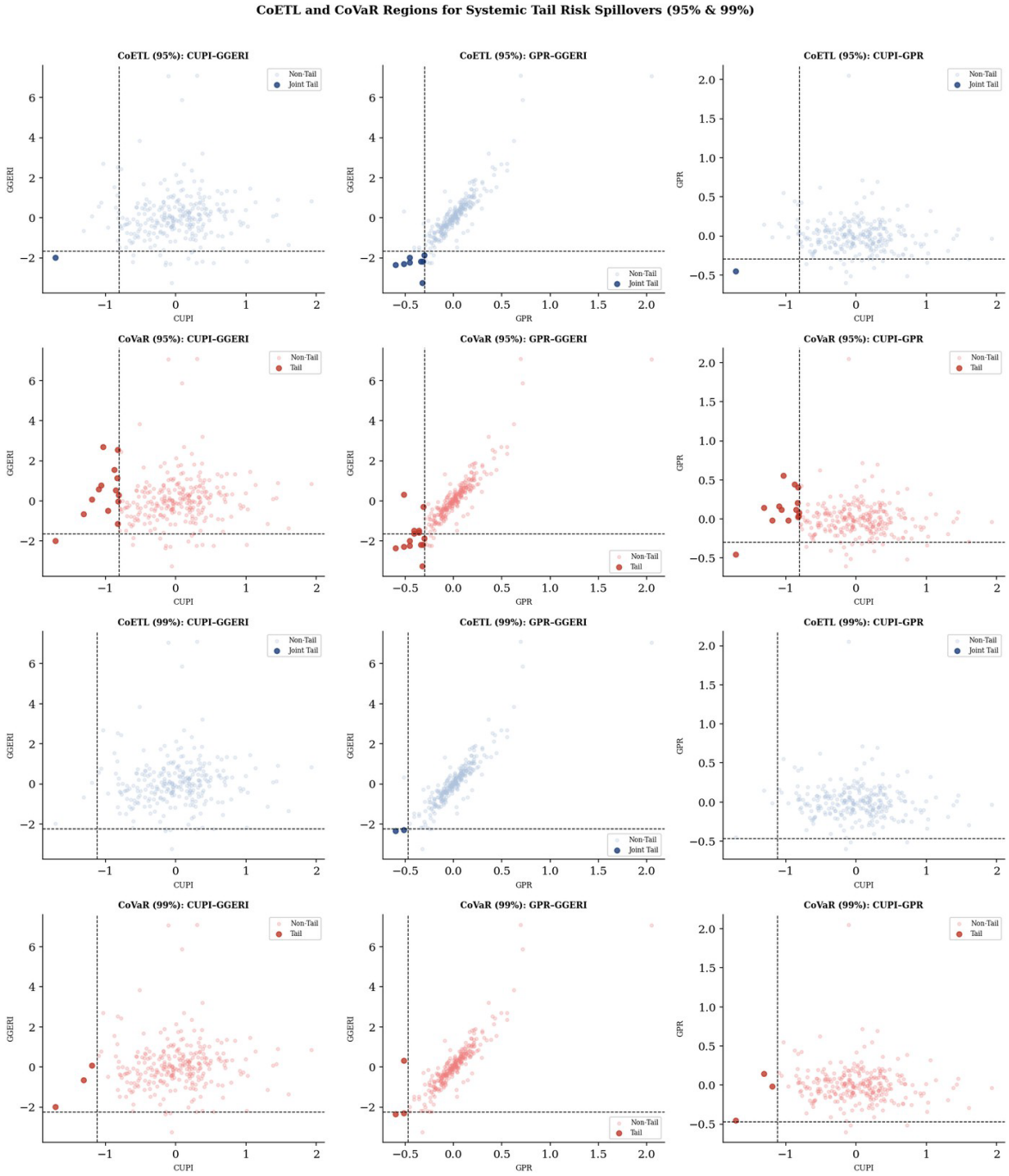


Figure 10: CoETL and CoVaR Regions for Systemic Tail Risk Spillovers at 95% and 99% Confidence Levels. Blue dots: joint tail regions (CoETL, defined by simultaneous breaches of both series' VaR thresholds). Red dots: conditional tail regions (CoVaR, where conditioning series exceeds its VaR threshold). Dashed lines mark the respective VaR thresholds. Panels organized by pair and confidence level.

5 Structural Regime Analysis

The heavy-tailed, right-skewed, and volatility-clustered properties of GGERI returns suggest that a single distributional regime is insufficient. We estimate a two-component Gaussian mixture model as a tractable approximation to a Hamilton (1989) Markov-switching framework:

$$f(r_t) = \pi_1 \, \varphi(r_t;\, \mu_1, \sigma_1) + \pi_2 \, \varphi(r_t;\, \mu_2, \sigma_2), \qquad \pi_1 + \pi_2 = 1, \tag{14}$$

where $\varphi(\,\cdot\,;\, \mu_k, \sigma_k)$ denotes the Gaussian density for regime k. Parameters are estimated by the EM algorithm with 10 random restarts; the BIC confirms two components as the preferred specification.

The estimated parameters identify two economically distinct regimes:

Low-risk regime ($k = 1$): $\hat{\mu}_1 = 0.776$, $\hat{\sigma}_1 = 2.385$, $\hat{\pi}_1 = 0.149$ ($\approx 15\%$ of months). Captures rare risk-abatement episodes (diplomatic breakthroughs, post-conflict resolution, successful climate summits) with positive mean return and high volatility from the heterogeneity of stabilization episodes.

High-risk regime ($k = 2$): $\hat{\mu}_2 = -0.058$, $\hat{\sigma}_2 = 0.796$, $\hat{\pi}_2 = 0.851$ ($\approx 85\%$ of months). Dominant background state of global systemic risk in the post-2000 era, characterized by a near-zero mean and lower volatility.

Figure 11 confirms that the high-risk regime is the persistent background state of global dual-risk in the post-2000 era - it accounts for roughly five out of every six months in the sample. Low-risk episodes are rare and heterogeneous: they cluster around the mid-2000s window of relative geopolitical calm and select months in 2013–2014 when both GPR and climate policy uncertainty were temporarily subdued. What makes this finding consequential for portfolio management is not the existence of two regimes but their extreme asymmetry. Decision-makers who calibrate risk models on full-sample average behavior implicitly assume a mixture of calm and turbulent conditions; in practice, they are almost always operating in the turbulent state. A risk framework anchored to the high-risk regime's parameters - higher tail thickness, more persistent volatility, stronger conditional co-movement between GPR and GGERI - will produce materially more conservative, and more accurate, assessments of downside exposure. The structural coupling that keeps the system in the high-risk regime is not accidental: in the post-Cold War multipolar order, geopolitical frictions have been endemic, while the green transition has made climate policy uncertainty a permanent feature of the macroeconomic landscape (Gavriilidis et al., 2026; Engle et al., 2020). Until both of



Figure 11: GGERI Returns with Markov-Switching Regime Identification (Jan 2001 – Dec 2023). *Upper panel:* Return bars colored by regime assignment (red: high-risk probability > 0.50; blue: low-risk). *Lower panel:* Filtered probability of the high-risk regime. Dashed horizontal line at 0.50 marks the classification threshold. Estimated parameters: Low-risk ($\hat{\mu}_1 = 0.776, \hat{\sigma}_1 = 2.385, \hat{\pi}_1 = 0.149$); High-risk ($\hat{\mu}_2 = -0.058, \hat{\sigma}_2 = 0.796, \hat{\pi}_2 = 0.851$).

these structural forces abate simultaneously - an event our regime model assigns roughly 15% unconditional probability - the high-risk regime should be treated as the operative baseline.

6 Derivative Pricing Applications

Consider the problem facing a portfolio manager who recognizes exposure to both geopolitical and climate-policy risk but finds that no single tradeable instrument captures both simultaneously. Purchasing a GPR-linked put provides event-driven protection but leaves the portfolio exposed to the slow-burning accumulation of climate regulatory uncertainty. A CUPI-linked instrument addresses the latter but is blind to discrete geopolitical shocks. GGERI-linked derivatives, by contrast, hedge the *joint* distribution - including the compounded tail events that are the most financially damaging precisely because they are not covered by either instrument alone.

To assess the derivative design implications of GGERI, we construct Black-Scholes implied volatility (IV) surfaces for CUPI, GPR, and GGERI separately, calibrated to the NIG parameters estimated from each series' return distribution. Comparing these surfaces reveals how the tails, asymmetry, and volatility persistence of each underlying manifest as option premia, and whether GGERI-linked derivatives would offer a materially different risk profile from their component alternatives. The IV surface is parameterized as a function of log-moneyness $m = \log(K/S)$ and maturity T:

$$\sigma_{\mathrm{IV}}(K, T) = \hat{\sigma}_{\mathrm{ann}} + \beta_1 \cdot m + \beta_2 \cdot m^2 + \gamma \cdot \tau(T) + \varepsilon, \qquad \tau(T) = \frac{1}{1 + 0.4\,T}, \tag{15}$$

where $\hat{\sigma}_{\mathrm{ann}}$ is the annualized realized volatility calibrated from each series' return distribution. The slope parameter $\beta_1 < 0$ captures the negative IV skew - the market's premium for downside protection - induced by the positive right skewness of the underlying returns under the risk-neutral measure; it is calibrated to the NIG asymmetry parameter $\hat{\beta}_{\mathrm{NIG}}$. The curvature parameter $\beta_2 > 0$ generates the smile shape driven by excess kurtosis - the additional premium at both tails relative to at-the-money options - calibrated to $\hat{\alpha}_{\mathrm{NIG}}$. The function $\tau(T)$ governs how the term structure of IV evolves with maturity, reflecting the intuition that volatility tends to revert toward a long-run level over longer horizons, compressing the spread between short- and long-dated IV. European call and put prices follow the standard

Black-Scholes formula:

$$C(S, K, T, r, \sigma) = S\,\Phi(d_1) - K\,e^{-rT}\,\Phi(d_2), \tag{16}$$

$$P(S, K, T, r, \sigma) = K\,e^{-rT}\,\Phi(-d_2) - S\,\Phi(-d_1), \tag{17}$$

$$d_{1,2} = \frac{\log(S/K) + (r \pm \frac{1}{2}\sigma^2)T}{\sigma\sqrt{T}}. \tag{18}$$

A key feature of the comparison across underlyings is the annualized volatility: CUPI carries a moderate level of annualized uncertainty, GPR carries less on a month-to-month basis (because large spikes are infrequent and mean-reverting), while GGERI - which standardizes, weights, and compounds both - carries substantially higher annualized volatility than either component. This hierarchy is not an artifact of construction; it reflects the genuine amplification that occurs when two independently heavy-tailed risk processes are aggregated into a single composite.

6.1 CUPI Implied Volatility Surface

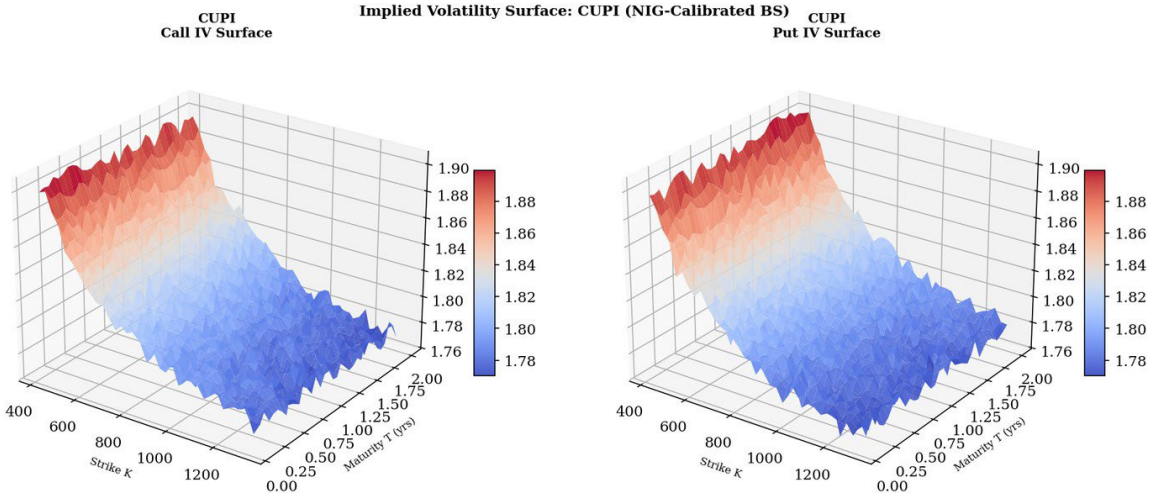


Figure 12: NIG-Calibrated Implied Volatility Surface for CUPI Underlying ($\hat{\sigma}_{\text{ann}} = 1.789$, $\beta_1 = -0.09$, $\beta_2 = 0.07$). Left panel: call IV surface. Right panel: put IV surface, both as functions of log-moneyness $m = \log(K/S)$ and maturity $T \in [1/12, 2]$ years. The mild negative skew and moderate smile curvature reflect CUPI's relatively symmetric return distribution - regulatory uncertainty tends to resolve gradually rather than in discrete, asymmetric jumps.

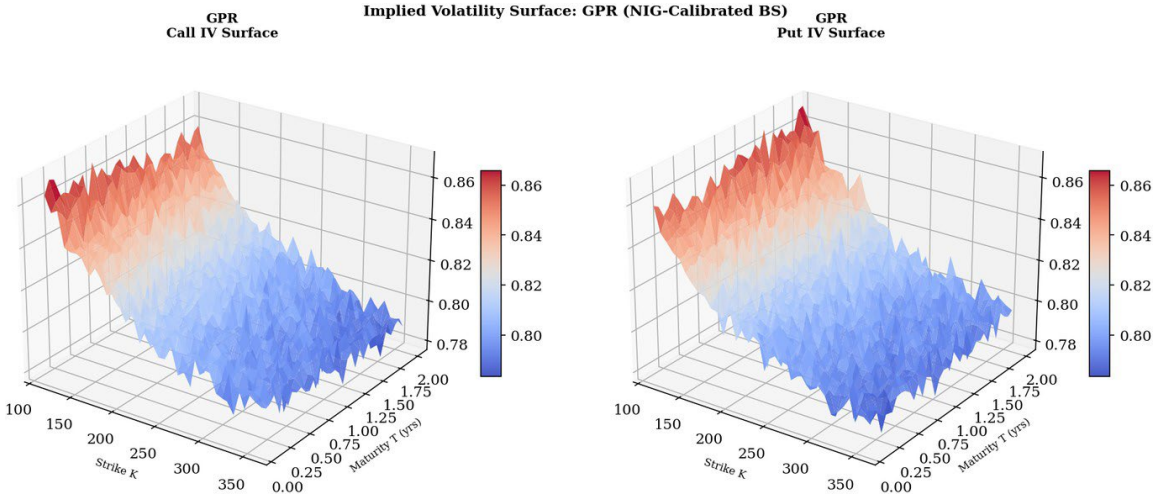


Figure 13: NIG-Calibrated Implied Volatility Surface for GPR Underlying ($\hat{\sigma}_{ann} = 0.795$, $\beta_1 = -0.05$, $\beta_2 = 0.03$). Left panel: call IV surface. Right panel: put IV surface. The relatively flat surface across maturities reflects the episodic, mean-reverting character of geopolitical risk: markets price near-term shocks at a premium but anticipate resolution over longer horizons, suppressing long-dated option premia.

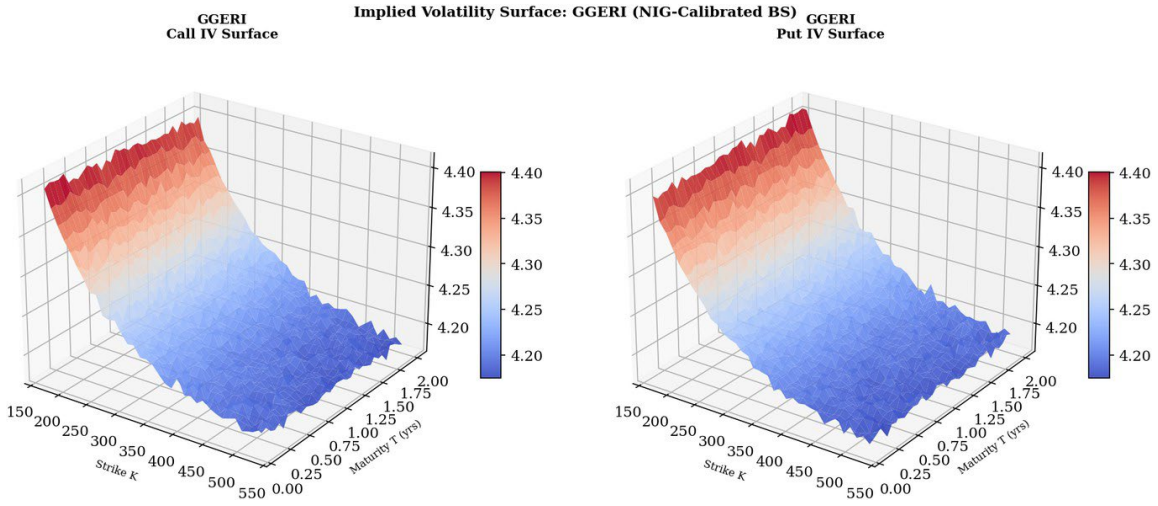


Figure 14: NIG-Calibrated Implied Volatility Surface for GGERI Underlying ($\hat{\sigma}_{ann} = 4.214$, $\beta_1 = -0.16$, $\beta_2 = 0.13$). Left panel: call IV surface. Right panel: put IV surface. The pronounced negative skew (left smirk) and steep smile curvature are calibrated to the NIG asymmetry and tail parameters estimated from the GGERI return series. The resulting surface is qualitatively indistinguishable from equity index volatility surfaces, suggesting that GGERI-linked options could plausibly be structured and traded within existing derivatives market infrastructure. Annualized volatility is more than five times that of GPR alone, reflecting the compounding of two persistent, heavy-tailed risk sources into a single underlying.

6.2 GPR Implied Volatility Surface

6.3 GGERI Implied Volatility Surface

Comparing the three IV surfaces, a clear decision-relevant hierarchy emerges. CUPI-based IV surfaces are relatively symmetric and moderate in curvature, consistent with a risk factor that moves persistently but not in dramatic discrete jumps. GPR-based surfaces exhibit a shallower smirk and flatter term structure, reflecting the market's intuition that most geopolitical crises eventually resolve: investors pay a premium for near-term protection but discount long-dated insurance. GGERI-based surfaces stand apart: the negative smirk is markedly steeper across all maturities, the smile curvature is larger, and the entire surface sits at a higher absolute volatility level. This is not merely a rescaling - it represents a qualitatively different options market that would price the *joint* probability of simultaneous geopolitical and climate-policy distress, precisely the scenario that investors most need to hedge and that single-index instruments fail to cover. To our knowledge, this is the first construction of an implied volatility surface anchored to a joint geopolitical-climate composite, and the proximity of GGERI's smirk structure to that of equity index options suggests it could be readily integrated into existing derivatives market infrastructure.

7 Conclusion

This paper develops, empirically validates, and explores the derivative pricing implications of the Global Geopolitical and Environmental Risk Index (GGERI) - a unified, dollar-denominated composite integrating the GPR (Caldara and Iacoviello, 2022) and CUPI (Gavriilidis et al., 2026) via rolling inverse-variance weighting, using monthly data from January 2000 to December 2023 ($N = 275$ log-return observations).

Five principal empirical findings emerge. First, GGERI log returns exhibit pronounced non-normality - skewness of 1.80, excess kurtosis of 8.92, and GARCH$(1, 1)$-t persistence of 0.916 with degrees of freedom 2.85 - confirming that heavy-tailed NIG innovations and near-integrated volatility dynamics are necessary features of any credible GGERI model. Second, Hill estimation establishes GGERI carries heavier tails ($\hat{\xi} \approx 0.81$) than either GPR (0.72) or CUPI (0.66), demonstrating that aggregation amplifies rather than diversifies tail risk. Third, Huber robust regression reveals GPR as the dominant linear driver at monthly frequency (slope $= 4.84$ vs. CUPI's 0.25). Fourth, $\mathrm{CoVaR} = -2.664$ and $\mathrm{CoETL} = -2.293$ at the 95% level for the GPR–GGERI pair confirm significant tail spillovers, while near-zero linear correlation ($\hat{\rho} = -0.073$) underscores the inadequacy of correlation-based dependence

measures. Fifth, a Gaussian mixture regime model identifies a persistent high-risk regime ($\hat{\pi} = 0.85$) as the background state of global dual-risk in the post-2000 era.

The NIG-calibrated IV surfaces demonstrate that GGERI-linked options exhibit equity-like negative volatility smirks with steeper skew ($\beta_1 = -0.16$) and higher smile curvature ($\beta_2 = 0.13$) than either GPR or CUPI alternatives, driven by GGERI's compounded tail structure ($\hat{\sigma}_{\text{ann}} = 4.214$). These characteristics motivate GGERI-linked puts and risk reversals as effective macro-hedging instruments for dual systemic risk exposure.

Limitations include the monthly frequency constraint, text-based CUPI construction that may miss emerging climate narratives, and USD denomination. Future research could incorporate physical climate risk indicators, apply higher-frequency text-based measures, explore multi-country GGERI variants, and develop full no-arbitrage stochastic volatility extensions for dynamic derivative pricing.

References

Adeabah, D. and Pham, T.P. (2025). Asymmetric tail risk spillover and co-movement between climate risk and the international energy market. *Energy Economics*, 141, 108122.

Adrian, T. and Brunnermeier, M.K. (2016). CoVaR. *American Economic Review*, 106(7), 1705–1741.

Ahmed, R., Chen, X.H., Hoang, Y.H., and Do-Linh, C. (2024). Climate change effects and their implications for the financial markets: Evidence from the United Kingdom. *Journal of Environmental Management*, 366, 121782.

Baker, S.R., Bloom, N., and Davis, S.J. (2016). Measuring economic policy uncertainty. *Quarterly Journal of Economics*, 131(4), 1593–1636.

Barndorff-Nielsen, O.E. (1997). Normal inverse Gaussian distributions and stochastic volatility modelling. *Scandinavian Journal of Statistics*, 24(1), 1–13.

Baur, D.G. and Smales, L.A. (2020). Hedging geopolitical risk with precious metals. *Journal of Banking and Finance*, 117, 105823.

Bedowska-Sójka, B., Demir, E., and Zaremba, A. (2022). Hedging geopolitical risks with different asset classes: A focus on the Russian invasion of Ukraine. *Finance Research Letters*, 50, 103192.

Billio, M., Getmansky, M., Lo, A.W., and Pelizzon, L. (2012). Econometric measures of

connectedness and systemic risk in the finance and insurance sectors. *Journal of Financial Economics*, 104(3), 535–559.

Brogaard, J., Dai, L., Ngo, P.T.H., and Zhang, B. (2020). Global political uncertainty and asset prices. *Review of Financial Studies*, 33(4), 1737–1780.

Caldara, D. and Iacoviello, M. (2022). Measuring geopolitical risk. *American Economic Review*, 112(4), 1194–1225.

Cheng, L., Qiu, R.-X., Zhao, L.-T., and Qu, Z. (2025). How do external uncertainties impact connectedness among carbon, fossil and clean energy markets? *Journal of Cleaner Production*, 498, 145200.

Choi, S. and Havel, J. (2025). Geopolitical risk and U.S. foreign portfolio investment. *Journal of International Money and Finance*, 151, 103253.

Demiralay, S., Wang, Y., and Chen, C. (2024). Geopolitical risks and climate change stocks. *Journal of Environmental Management*, 352, 119995.

DeMiguel, V., Garlappi, L., and Uppal, R. (2009). Optimal versus naive diversification: How inefficient is the $1/N$ portfolio strategy? *Review of Financial Studies*, 22(5), 1915–1953.

Engle, R.F., Giglio, S., Kelly, B., Lee, H., and Stroebel, J. (2020). Hedging climate change news. *Review of Financial Studies*, 33(3), 1184–1216.

Gala, V.D., Pagliardi, G., and Zenios, S.A. (2023). Global political risk and international stock returns. *Journal of Empirical Finance*, 72, 78–102.

Gavriilidis, K., Känzig, D.R., Raghavan, M., and Stock, J. (2026). Climate policy uncertainty and sentiment dataset. Working paper.

Giglio, S., Kelly, B., and Stroebel, J. (2021). Climate finance. *Annual Review of Financial Economics*, 13, 15–36.

Hamilton, J.D. (1989). A new approach to the economic analysis of nonstationary time series and the business cycle. *Econometrica*, 57(2), 357–384.

Hill, B.M. (1975). A simple general approach to inference about the tail of a distribution. *Annals of Statistics*, 3(5), 1163–1174.

Ji, Q., Ma, D., Zhai, P., Fan, Y., and Zhang, D. (2024). Global climate policy uncertainty and financial markets. *Journal of International Financial Markets, Institutions and Money*, 95, 102047.

Jin, Y., Zhao, H., Bu, L., and Zhang, D. (2023). Geopolitical risk, climate risk and energy markets: A dynamic spillover analysis. *International Review of Financial Analysis*, 87, 102597.

Kan, R. and Zhou, G. (2007). Optimal portfolio choice with parameter uncertainty. *Journal of Financial and Quantitative Analysis*, 42(3), 621–656.

Liu, Z., Wang, Y., Yuan, X., Ding, Z., and Ji, Q. (2025). Geopolitical risk and vulnerability of energy markets. *Energy Economics*, 141, 108055.

Ma, F., Cao, J., Wang, Y., Vigne, S.A., and Dong, D. (2023). Dissecting climate change risk and financial market instability. *Risk Analysis*, 44(3), 618–635.

Shirvani, A., Mittnik, S., Lindquist, W.B., and Rachev, S.T. (2024). Bitcoin volatility and intrinsic time using double-subordinated Lévy processes. *Risks*, 12(5), 82.

Smales, L.A. (2021). Geopolitical risk and volatility spillovers in oil and stock markets. *Quarterly Review of Economics and Finance*, 80, 358–366.

Trindade, A., Shirvani, A., and Ma, X. (2020). A socioeconomic well-being index. *Applied Economics and Finance*, 7(4), 48–62.

Umar, Z., Bossman, A., Choi, S.Y., and Teplova, T. (2022). Does geopolitical risk matter for global asset returns? Evidence from quantile-on-quantile regression. *Finance Research Letters*, 48, 102991.

Xie, Q., Bi, Y., Xi, Y., and Xu, X. (2025). The impact of geopolitical risk on higher-order moment risk spillovers in global energy markets. *Energy Economics*, 144, 108292.

Yilmazkuday, H. (2024). Geopolitical risk and stock prices. *European Journal of Political Economy*, 83, 102553.

Zaremba, A., Cakici, N., Demir, E., and Long, H. (2022). When bad news is good news: Geopolitical risk and the cross-section of emerging market stock returns. *Journal of Financial Stability*, 58, 100964.

Zhang, T., Xu, H.-C., and Zhou, W.-X. (2025). The impact of external uncertainties on the extreme return connectedness between food, fossil energy, and clean energy markets. Working paper, arXiv:2503.06603.

Zhang, Y., He, J., He, M., and Li, S. (2023). Geopolitical risk and stock market volatility: A global perspective. *Finance Research Letters*, 53, 103620.